Polymer Chemistry

PAPER

View Article Online
View Journal | View Issue

Cite this: *Polym. Chem.*, 2015, **6**, 3728

Influences of the backbone randomness on the properties, morphology and performances of the fluorinated benzoselenadiazole–benzothiadiazole based random copolymers†

Yung-Tsung Chen, Tzu-Wei Huang, Chien-Lung Wang* and Chain-Shu Hsu*

Received 4th February 2015, Accepted 31st March 2015

DOI: 10.1039/c5py00175g

www.rsc.org/polymers

To investigate the influences of the 5,6-difluoro-benzoselenadiazole : 5,6-difluoro-benzothiadiazole (**FBSe** : FBT) ratio on the polymer properties, solid-state morphology and device performances, a series of **FBSe** : FBT based copolymers were synthesized. Copolymers with higher **FBSe** ratios were found to have narrower E_g, and higher-lying E_{HOMO}. Because of the size and electronegativity differences of the selenium and sulfur atoms, the **FBSe** : FBT ratio further affects the structural regularity of the conjugated chains, and their self-assembly behaviors. DSC results indicated that **P1**, which has the most irregular **FBSe** : FBT sequence along the backbone showed the lowest T_m. Interestingly, XRD results showed that the main-chain irregularity degrades the order of the lamellar stacking, but not the order of π-stacking. The random ternary copolymers, **P1** and **P2**, possess more ordered π-stacking than the alternating copolymers, **PTh$_4$FBSe** and **PTh$_4$FBT**. The highest OFET μ_h of 0.46 cm^2 V^{-1} s^{-1} was delivered by **P1**, which has the smallest $d_{\pi-\pi}$ among the copolymers. In the polymer : PC$_{71}$BM blend films, the **FBSe** containing copolymers have good miscibility in PC$_{71}$BM. The degree of phase separation of **PTh$_4$FBSe** : PC$_{71}$BM can be enhanced by DIO additive, but it is not effective for the random ternary copolymers. The highest PCE of 6.06% with V_{oc} of 0.64 V, J_{sc} of 15.3 mA cm^{-2}, and FF of 61.8% was delivered by the **PTh$_4$FBSe** : PC$_{71}$BM PSCs.

Introduction

Low band-gap (LBG) conjugated copolymers consisting of an electron-rich donor unit (D) and an electron-deficient acceptor unit (A) have been developed as high-performance materials used in bulk heterojunction (BHJ) polymer solar cells (PSCs).[1–5] Rapid developments in the polymer design enabled the adjustments of the highest occupied molecular orbital level (E_{HOMO}) and the lowest unoccupied molecular orbital level (E_{LUMO}) of the LBG copolymers. Combining the suitable E_{HOMO} and E_{LUMO} of the LBG copolymer, appropriate device design and morphological optimization, BHJ PSCs have reached power conversion efficiencies (PCEs) over 8%.[6–19]

Recently, random copolymerization has been developed as a versatile strategy to further adjust the properties of D–A copolymers. The D–A random copolymers were generally prepared either by copolymerizing two different D units with one A unit,[19–22] or by copolymerizing two different A units with one D unit.[23–29] Compared to the alternating D–A copolymers, which contain only two monomeric units, the additional monomeric units in the ternary random copolymers provide extra flexibility to adjust the polymer properties. Different ternary random copolymers have been synthesized to either broaden the absorption spectrum,[19] modulate the E_{HOMO} and E_{LUMO} positions,[23] or to control the solid-state morphology.[22] Over 7% PCEs have been reported in the single-junction BHJ PSCs of several random D–A copolymers, and a PCE of over 8.5% has also been reported in our previous study using the prophyrin-containing random copolymers.[19]

Although the versatility of random copolymerization has been confirmed, because the reaction brings both irregularity to the chemical structure and randomness to the chain sequence along the conjugated backbone, fundamental questions about how these molecular parameters influence the solid-state morphology and device performances of the random D–A copolymers remain an interesting issue to be explored. A suitable acceptor pair for the study of the influences of the backbone randomness is fluorinated benzothiadiazole (FBT) and fluorinated benzoselenadiazole (**FBSe**). Unlike most ternary random copolymers containing two A units with very different structures, **FBSe** and FBT have very similar chemical structures. Thus, when randomly copolymer-

Department of Applied Chemistry, National Chiao Tung University, 1001Ta Hsueh Rd., Hsinchu, Taiwan 30010. E-mail: cshsu@mail.nctu.edu.tw, kclwang@nctu.edu.tw

†Electronic supplementary information (ESI) available. See DOI: 10.1039/c5py00175g

ized, the overall chemical structure of the random copolymers will not be significantly altered with the **FBSe** : FBT ratios. However, because the selenium atom (Se) and the sulfur atom (S) are different in their electronegativity and sizes,[30–35] changing the **FBSe** : FBT ratio in the ternary random copolymers can still change the polymer properties and bring the sequential randomness into the conjugated backbone. In general, the **FBSe**-based copolymers[36–38] have smaller E_g,[39–42] but higher-lying E_{HOMO} than the FBT-based copolymers,[43–46] because the Se-containing unit is more polarized than its S analogue and possesses more quinoidal character.[47] Currently, the **FBSe**-based copolymers have delivered a promising PCE of 5.74% in the literature. Adjusting the FBT/**FBSe** ratio in a ternary random copolymer may optimize the polymer properties, and provide information about how the backbone randomness affects the solid-state structures of the random copolymers. Thus, in this study, a series of LBG copolymers, which contain **FBSe** and FBT as a pair of A units and 5,5′-dibromo-4,4′-bis-(2-octyldodecyl)-2,2′-bithiophene as the D unit, were synthesized to investigate the influences of the **FBSe** : FBT ratio on the polymer properties, solid-state behaviors and device performances. As shown in Scheme 1, the **FBSe** : FBT ratios are 100 : 0 for **PTh$_4$FBSe**, 50 : 50 for **P1**, and 25 : 75 for **P2**. UV-Vis spectra and electrochemical cyclic voltammetry (CV) were used to evaluate influences of the **FBSe** : FBT ratio on the E_{HOMO}, E_{LUMO} and E_g. The phase behavior and the phase structure of the copolymers were investigated by differential scanning calorimetry (DSC) and X-ray diffractometry. The morphology of the copolymer/PCBM blend films and the influences of the diiodooctane (DIO) additive were observed by transmission electron microscopy (TEM). The **FBSe** : FBT ratio showed obvious influences on the properties and solid-state morphologies of the copolymers. The highest OFET hole mobility (μ_h) of 0.46 cm^2 V^{-1} s^{-1} was delivered by **P1**, which has the smallest $d_{\pi-\pi}$, while the highest PCE of 6.06% with V_{oc} of 0.64 V, J_{sc} of 15.3 mA cm^{-2}, and FF of 61.8% was delivered by the **PTh$_4$FBSe** : PC$_{71}$BM PSCs because of the suitable degree of phase segregation in the blend thin film.

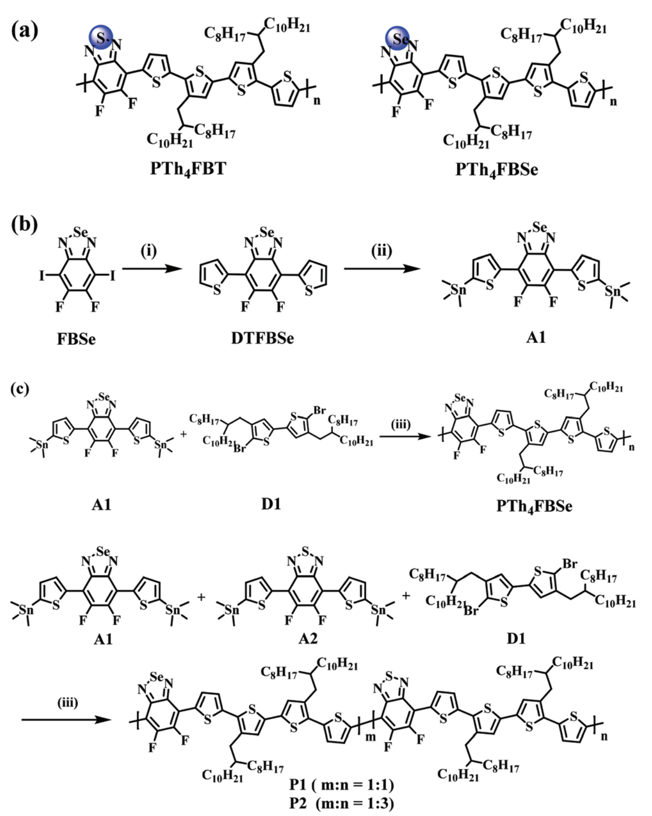

Scheme 1 (a) Chemical structures of **PTh$_4$FBT** and **PTh$_4$FBSe**. (b), (c) Synthetic procedures and conditions of the monomers and copolymers: (i) 2-(tributylstannyl)thiophene, tetrakis (triphenylphosphine)palladium(0), DMF, 120 °C, 24 h; (ii) LDA, dry THF, −78 °C, 1 h; 1 M trimethyltin chloride; (iii) tris(dibenzylideneacetone)dipalladium(0), tri(*o*-tolyl)phosphine, chlorobenzene, 180 °C, microwave 270 W, 50 min.

Experimental section

General measurement and characterization

All chemicals were purchased from Aldrich, Lancaster, TCI or Acros and used as received unless otherwise specified. ^{1}H and ^{13}C NMR spectra were recorded using a 400 and 75 MHz instrument spectrometer. Differential scanning calorimetry (DSC) was performed on a TAQ200 Series DSC operated at a scan rate of 10 °C min^{-1}. Thermogravimetric analysis (TGA) was performed using a Perkin Elmer Pyris under a nitrogen atmosphere at a heating rate of 10 °C min^{-1}. UV-Vis spectra were recorded using an HP 8453 spectrophotometer. The electrochemical cyclic voltammetry (CV) was conducted on a CH Instruments Model 611D. Carbon glass coated with a thin polymer film was used as the working electrode and the Ag/Ag$^+$ electrode as the reference electrode, while 0.1 M tetrabutylammoniumhexafluorophosphate (Bu$_4$NPF$_6$) in acetonitrile was the electrolyte. CV curves were calibrated using ferrocene as the standard, whose oxidation potential is set at −4.8 eV with respect to the zero vacuum level. The E_{HOMO} were deduced from the equation: $E_{HOMO} = -e(E_{ox}^{onset} - E_{(ferrocene)}^{onset} + 4.8)$ eV. The E_{LUMO} levels of the polymer were deduced from the equation: $E_{LUMO} = -e(E_{red}^{onset} - E_{(ferrocene)}^{onset} + 4.8)$ eV. For X-ray diffraction (XRD) patterns, a Bruker APEX DUO Single Crystal X-Ray Diffractometer with a microfocus air-cooled sealed Cu tube source, 50 watts, (50 kV, 1 mA; K$_\alpha$ radiation 0.1542 nm) and an APEXII CCD camera was used. For the 2D WAXD analysis, the fiber samples were prepared by extruding the polymers through a pin-hole (diameter: 1 mm) at 200 °C. The fiber samples were then exposed to the X-ray (beam size: 0.3 mm). The exposure time to obtain high-quality patterns was 40 seconds.

OFET device fabrication and characterization

An n-type heavily doped Si wafer with a SiO$_2$ layer of 300 nm and a capacitance of 11 nF cm^{-2} was used as the gate electrode and a dielectric layer. Thin films (40–60 nm in thickness) of polymers were deposited on ODTS treated SiO$_2$/Si substrates by spin-coating their *o*-DCB solution (5 mg mL^{-1}). The thin films were annealed at 200 °C or 250 °C for 10 minutes. A gold source and drain contacts (40 nm in thickness) were deposited by vacuum evaporation on the organic layer through a shadow mask, affording a bottom-gate, top-contact OFET device. Electrical measurements of the OFET devices were carried out at room temperature in air using a 4156C Semiconductor Parameter Analyzer, Agilent Technologies. The field-effect mobility was calculated in the saturation regime by using the equation: $I_{ds} = (\mu WC_i/2L)(V_g - V_t)^2$, where I_{ds} is the drain-source current, μ is the field-effect mobility, W is the channel width (1 mm), L is the channel length (0.1 mm), C_i is the capacitance per unit area of the gate dielectric layer, V_g is the gate voltage and V_t is the threshold voltage.

BHJ PSC fabrication and characterization

The device structure for inverted PSCs was ITO/ZnO/polymer : $PC_{71}BM/MoO_3$/Ag. The ITO glass substrates were cleaned with detergent, deionized water, acetone, and isopropyl alcohol in an ultrasonic bath and then dried overnight in an oven at >100 °C. For the inverted PSCs, zinc acetate dihydrate (Aldrich) dissolved in 2-methoxyethanol (100 mg mL^{-1}) and a small amount of ethanolamine was spin-casted on pre-cleaned ITO substrates and baked at 160 °C for 10 minutes in air to form the ZnO layer with a thickness of 40 nm. Copolymers were dissolved in chlorobenzene (CB) containing 3 vol% DIO. $PC_{71}BM$ (purchased from Nano-C) was then added into the solution to reach the desired weight ratio. The solution was stirred at 70 °C overnight and filtered through a 0.45 μm filter. In a glove box, the solution of polymer : $PC_{71}BM$ was then spin coated to form the active layer. The anode made of MoO_3 (7 nm) and Ag (150 nm) was evaporated through a shadow mask under vacuum (<10^{-6} Torr). Each sample consisted of four independent pixels defined by an active area of 0.04 cm^2. The devices were characterized in air under 100 mW cm^{-2} AM 1.5 simulated light measurement (Yamashita Denso solar simulator). Current–voltage (*J*–*V*) characteristics of PSC devices were obtained by using a Keithley 2400 SMU. Solar illumination conforming to the JIS Class AAA was provided by using a SAN-EI 300W solar simulator equipped with an AM 1.5G filter. The light intensity was calibrated with a Hamamatsu S1336-5BK silicon photodiode.

Transmission electron microscopy (TEM)

TEM observations were performed in bright-field, high-resolution mode on a JEOL JEM-2010 transmission electron microscope with an accelerating voltage of 200 kV equipped with a Gatan-831 CCD camera. The thin-film sample was first spin-coated onto an ITO substrate covered with 40 nm of PEDOT : PSS. The sample was then immersed in water to dissolve the PEDOT : PSS layer and separate the thin films from the ITO substrate. Thin films floated on a water surface were picked up by copper grids coated with an amorphous carbon layer, dried under vacuum overnight, and used in the TEM observations.

Synthesis of DTFBSe

To a round bottom flask were added 5,6-difluoro-4,7-diiodobenzo-2,1,3-selenadiazole (1.5 g, 3.18 mmol), $Pd(PPh_3)_4$ (290 mg, 0.251 mmol) and degassed DMF (50 mL). The solution was stirred at 60 °C until all the substances completely dissolved. 2-(Tributylstannyl)thiophene (2.76 g, 7.4 mmol) was added dropwise and the mixture was kept at 120 °C for 20 h. Then, the mixture was poured into water and extracted with dichloromethane, before being dried over anhydrous $MgSO_4$. After concentration, the residue was purified by column chromatography using hexane and dichloromethane (v/v = 4 : 1) as the eluent to afford an orange solid (0.66 g, yield 54%). ^1H NMR ($CDCl_3$, 400 MHz, δ): 7.27 (d, J = 4.8 Hz, 2H), 7.63 (d, J = 5.2 Hz, 2H), 8.18 (d, J = 4 Hz, 2H); ^{13}C NMR ($CDCl_3$, 75 MHz, δ): 112.38, 127.24, 129.04, 129.06, 129.08, 130.92, 130.97, 131.02, 131.70, 149.09, 149.31, 151.70, 151.92, 154.30; Anal. calcd for $C_{14}H_6F_2N_2S_2Se$: C 43.87, H 1.58, N 7.31; found: C 44.12, H 1.81, N 7.11.

Synthesis of 5,6-difluoro-4,7-bis(5-(trimethylstannyl)thiophen-2-yl)benzo-2,1,3-selenodiazole (A1)

To a solution of compound **DTFBSe** (320 mg, 0.83 mmol) in dry THF (50 mL) was added a 2 M solution of lithium diisopropylamide in THF (1.08 mL, 2.16 mmol) dropwise at −78 °C. After stirring at −78 °C for 1 h, a 1.0 M solution of chlorotrimethylstannane in THF (2.16 mL, 2.16 mmol) was introduced by syringe into the solution. The mixture solution was warmed up to room temperature and stirred for 20 h. The mixture solution was extracted with diethyl ether (50 mL × 3) and water (50 mL). The solvent was evaporated under reduced pressure and the product was obtained by recrystallization from methanol. Yield: 300 mg (51%). ^1H NMR ($CDCl_3$, 400 MHz, δ): 0.44 (s, 18H), 7.34 (d, J = 3.6 Hz, 2H), 8.22 (d, J = 3.6 Hz, 2H).

Synthesis of PTh_4FBSe

To a 50 mL round bottom flask were added compound **A1** (85.3 mg, 0.129 mmol), 5,5′-dibromo-4,4′-bis(2-octyldodecyl)-2,2′-bithiophene (**D1**) (114 mg, 0.129 mmol), tris(dibenzylideneacetone)dipalladium (5.9 mg, 0.0065 mmol), tri(2-methylphenyl)phosphine (15.7 mg, 0.052 mmol) and deoxygenated chlorobenzene (5 mL). The mixture was then degassed by bubbling nitrogen for 10 minutes at room temperature. The round bottom flask was put into the microwave reactor and heated to 180 °C under 270 watts for 50 minutes. Then, tributyl(thiophen-2-yl)stannane (10.5 mg, 0.028 mmol) was added to the mixture solution and reacted for 10 minutes under 270 W. Finally, 2-bromothiophene (20 mg, 0.123 mmol) was added to the mixture solution and reacted for 10 minutes under 270 W. After cooling to room temperature the solution was added dropwise to methanol. The precipitate was collected by filtration and washed by Soxhlet extraction with acetone (24 h) and hexane (24 h) sequentially. The residue solid was re-dissolved in hot toluene (100 mL). The Pd-thiol gel (Silicycle Inc.) was added to the above toluene solution to remove the residual Pd catalyst at 60 °C for 12 h. After filtration of the solution and removal of the solvent under reduced pressure, the polymer solution was added into methanol to re-precipitate. The purified polymer was collected by filtration and dried under vacuum for 1 day to give a black solid. Yield: 100 mg (50.2%). ^{1}H NMR ($CDCl_3$, 400 MHz, δ): 0.86 (br, 12H), 1.25 (br, 64H), 1.77 (br, 2H), 2.78 (br, 4H), 6.98–7.01 (br, 4H), 8.16 (br, 2H); Anal. calcd: C 67.29, H 8.02, N 2.53, S 11.59; found: C 66.76, H 7.34, N 2.66, S 11.75.

Synthesis of P1

Using a procedure similar to that described above for **PTh$_4$FBSe**, a mixture of **A1** (43.04 mg, 0.06 mmol), **A2** (40.2 mg, 0.06 mmol), **D1** (107.5 mg, 0.12 mmol), tris(dibenzylideneacetone)dipalladium (5.56 mg, 0.0061 mmol), tri-(2-methylphenyl)phosphine (14.8 mg, 0.049 mmol) in deoxygenated chlorobenzene (5 mL) was polymerized to give **P1**. Yield: 63 mg (47.8%). ^{1}H NMR ($CDCl_3$, 400 MHz, δ): 0.86 (br, 12H), 1.26 (br, 64H), 1.77 (br, 2H), 2.79 (br, 4H), 6.98–7.03 (br, 4H), 8.17–8.29 (br, 2H); Anal. calcd: C 68.75, H 8.19, N 2.59, S 13.32; found: C 67.24, H 7.50, N 2.81, S 13.35.

Synthesis of P2

Using a procedure similar to that described above for **PTh$_4$FBSe**, a mixture of **A1** (18.52 mg, 0.026 mmol), **A2** (51.88 mg, 0.078 mmol), **D1** (92.85 mg, 0.104 mmol), tris-(dibenzylideneacetone)dipalladium (5.56 mg, 0.0061 mmol), tri(2-methylphenyl)phosphine (14.8 mg, 0.049 mmol) in deoxygenated chlorobenzene (5 mL) was polymerized to give **P2**. Yield: 62 mg (55.1%). ^{1}H NMR ($CDCl_3$, 400 MHz, δ): 0.86 (br, 12H), 1.26 (br, 64H), 1.77 (br, 2H), 2.79 (br, 4H), 6.98–7.04 (br, 4H), 8.18–8.29 (br, 2H); Anal. calcd: C 69.53, H 8.28, N 2.61, S 14.25; found: C 69.48, H 7.84, N 2.80, S 14.44.

Results and discussion

Synthesis and thermal analysis

As shown in Scheme 1, to obtain the **FBSe** alternating copolymer (**PTh$_4$FBSe**) and the **FBSe** : FBT ternary random copolymers (**P1** and **P2**), the monomer 5,6-difluoro-4,7-bis-(5-(trimethylstannyl)thiophen-2-yl)benzo-2,1,3-selenodiazole (**A1**) was first synthesized according to Scheme 1b. The Stille-coupling of 5,6-difluoro-4,7-diiodobenzo-2,1,3-selenodiazole and 2-(tributylstannyl)thiophene afforded the formation of **DTFBSe** in 68% yield. **A1** was synthesized by reacting the lithiated **DTFBSe** with trimethyltin chloride in 54% yield. 5,6-Difluoro-4,7-bis(5-(trimethylstannyl)thiophen-2-yl)benzo-2,1,3-thiadiazole (**A2**) and 5,5′-dibromo-4,4′-bis(2-octyldodecyl)-2,2′-bithiophene (**D1**) were synthesized *via* reported methods.[48] Then, **PTh$_4$FBSe** was synthesized by the copolymerization between **A1** and **D1** *via* Stille coupling. The ternary random copolymers, **P1** and **P2**, were prepared by the copolymerization of the mixtures of **A1**, **A2** and **D1**. The molar ratios were **A1** : **A2** : **D1** = 1 : 1 : 2 for **P1** and **A1** : **A2** : **D1** = 1 : 3 : 4 for **P2**. The **FBSe** : FBT feed ratios of **PTh$_4$FBSe**, **P1** and **P2** are thus 100 : 0, 50 : 50 and 25 : 75. The sulfur content in the polymers obtained from the elemental analysis is 11.75% for **PTh$_4$FBSe**, 13.35% for **P1** and 14.25% for **P2**. The content closely matches with the calculated values and gives a clear indication about the **FBSe** : FBT ratios of the copolymers. The copolymers (**PTh$_4$FBSe**, **P1** and **P2**) were completely soluble in chloroform, chlorobenzene (CB), and *o*-dichlorobenzene (*o*-DCB). The number average molecular weights (M_n) of **PTh$_4$FBSe** and **P1** were 15.4 kDa (PDI = 1.72) and 12.3 kDa (PDI = 1.83), respectively, as determined by gel permeation chromatography (GPC). The molecular weight of **P2** was not obtainable from the GPC measurement due to its poor solubility in THF.

PTh$_4$FBSe, **P1** and **P2** exhibited good thermal stability with decomposition temperature (T_d) around 400 °C determined from thermogravimetric analysis (Fig. S2†). In the DSC analysis (Fig. S3†), the melting temperature (T_m) of **PTh$_4$FBSe**, **P1** and **P2** is 259 °C, 251 °C and 272 °C, respectively. The transition peaks of **PTh$_4$FBSe** and **P2** are also sharper than that of **P1**. The different phase behaviors of the copolymers are related to the **FBSe** : FBT ratio. The highest T_m of **P2** suggests that a higher FBT content prompts the T_m of the copolymer. Moreover, the **FBSe**/FBT sequence along the conjugated backbone has a non-negligible effect on the phase stability. Although **P1** has a higher FBT ratio than **PTh$_4$FBSe**, its broad phase transition at lower temperatures indicates that the backbone randomness decreases the transition temperature and the stability of the ordered phase.

Optical absorption and frontier orbital levels

Fig. 1 displays the UV-Vis absorption spectra of the copolymers in *o*-DCB and thin films; Table 1 summarizes the optical data, including the absorption peak wavelengths (λ_{max}s), absorption edges (λ_{onset}s), and optical band gaps (E_gs) of the copolymers. In solution (Fig. 1a), the absorption bands at λ_{max} around

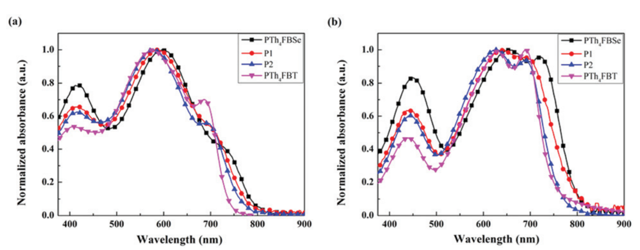

Fig. 1 Normalized (a) solution in *o*-DCB and (b) thin-film UV-vis absorption spectra of the copolymers.

Table 1 Optical and electrochemical properties of copolymers

Polymer	λ_{max} (nm) Solution	Film	λ_{onset} (nm)	E_g (eV)	E_{HOMO} (eV)	E_{LUMO} (eV)
PTh$_4$FBSe	600	656, 721	798	1.55	5.27	3.80
P1	588	643, 695	791	1.57	5.31	3.72
P2	576	628, 687	761	1.62	5.35	3.70

420 nm can be attributed to the localized π–π* transitions and the absorption bands at λ_{max} around 580 nm were attributed to the photo-induced intramolecular charge transfer (ICT) between the electron-rich quaterthiophene units and electron-deficient FBT or **FBSe** units. As shown in Fig. 1b, the absorption bands bathochromically shift when the copolymers are spin-casted into the film. The low-energy absorption shoulders with λ_{max} located at 721 nm (**PTh$_4$FBSe**), 695 nm (**P1**) and 687 nm (**P2**) indicate a better backbone co-planarity and stronger intermolecular interactions of the conjugated chains in the thin film. The major influence of the **FBSe** : FBT ratio is on the E_g of the copolymer. Deduced from the absorption edges of the thin film spectra, the E_gs are 1.55 eV for **PTh$_4$FBSe**, 1.58 eV for **P1** and 1.62 eV for **P2**. Thus, a decrease in the **FBSe** content widens the E_g of the copolymers. Cyclic voltammetry (Fig. S1a†) was performed for each copolymer to obtain information about their E_{HOMO} and E_{LUMO} levels. The relevant electrochemical properties are summarized in Table 1. Comparing the E_{HOMO}s and E_{LUMO}s of the copolymers, it was found that the decreased **FBSe** content drops the E_{HOMO}, but elevates the E_{LUMO} of the copolymers as shown in Fig. S1b.† Thus, modulation of the E_{HOMO}s, E_{LUMO}s and E_gs of copolymers can be reached *via* the control of the **FBSe** : FBT ratio.

X-ray structural characterization

X-ray diffraction (XRD) analysis of the copolymers (Fig. 2) was carried out to identify how the **FBSe** : FBT ratio affects the solid-state packing of the copolymers. To give a comprehensive comparison, **PTh$_4$FBT** from our previous study[46] is also incorporated into the discussion. All copolymers form a long-range ordered lamellar structure (*d*-spacing of 2.07 nm), and ordered π–π stacking in the solid-state, as indicated by the three diffraction peaks indexed as the (100), (200), and (300) diffractions in a low angle region, and an additional diffraction at around 23.7° (*d*-spacing ~0.37 nm). The π–π stacking distances ($d_{\pi-\pi}$s) are 0.374 nm for **PTh$_4$FBSe** and **P2**; 0.368 nm for **P1**; and 0.370 nm for **PTh$_4$FBT**.

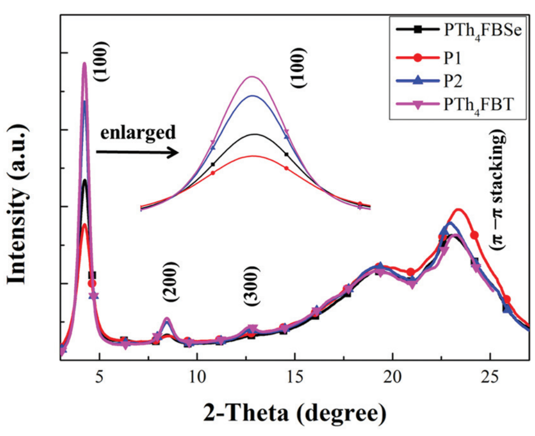

Fig. 2 Powder XRD patterns of the **FBSe** : FBT copolymers.

Fig. S5† shows the 2D WAXS pattern of the extruded samples. The chain axis (*c*-axis) of the copolymers is aligned along the shear direction. Therefore, the Bragg diffractions along the equator can be used to identify the diffractions from the lamellar structure (indexed as (100) in the figures), and the π–π stacking.[49] To make a reasonable comparison, the sample diameter was controlled by the size of the pinhole on the extruder (1 mm) and the exposure time was fixed for the four samples. The scattering halo from the alkyl side chains was clearly found at $2\theta = 19.2°$ (*d*-spacing of 0.47 nm). Because the four polymers have the same alkyl side chains, the scattering intensities from the amorphous side chains are similar in the four diffraction patterns shown in Fig. S5.† However, the integration of the diffraction peaks along the equator (Fig. S6†) shows the differences in the diffraction intensities of the (100) and π–π peaks of the four copolymers. For the (100) diffraction, the intensities of the copolymers are in the order of **PTh$_4$FBT** > **P2** > **PTh$_4$FBSe** > **P1**, and for the π–π diffraction, the intensity is in the order of **P1** > **P2** > **PTh$_4$FBSe** ~ **PTh$_4$FBT**. The result is in accordance with the powder XRD patterns shown in Fig. 2. Thus, the XRD results indicate that the **FBSe** : FBT ratio does not affect the lamellar spacing, but does influence the order of the lamellar structure and the $d_{\pi-\pi}$ of the copolymers. Copolymers with higher FBT content (**PTh$_4$FBT** and **P2**) generated sharper (100) diffractions than those with higher **FBSe** content. Since the sharpness of the diffraction is related to the correlation length of crystalline domain according to the Scherrer equation, the order of the lamellar structure is therefore lower in the copolymers with higher **FBSe** content (**PTh$_4$FBSe**) and higher backbone randomness (**P1**). However, to the π-stacking, the backbone randomness shows an opposite effect. The alternative copolymers – **PTh$_4$FBSe** and **PTh$_4$FBT** gave lower diffraction intensities for the π–π stacking than the random ternary copolymers – **P1** and **P2**. Moreover, **P1**, which has the most random backbone, gave the most intense π-stacking diffraction and the shortest $d_{\pi-\pi}$ of 0.368 nm. Because the four copolymers are different in their **FBSe** : FBT ratio, or more specifically speaking, in the content and the arrangement of the selenium (Se)/sulfur (S) atoms, the result was rational based on the steric effect of the Se atom and the intermolecular interaction strength of the **FBSe** unit. On the one hand, the atom size of Se is larger than S. Comparing the $d_{\pi-\pi}$ of **PTh$_4$FBSe** (0.374 nm) and **PTh$_4$FBT** (0.370 nm), it can be found that the larger atomic size of Se causes steric hindrance, and expands the $d_{\pi-\pi}$ of **PTh$_4$FBSe.**[50] On the other hand, due to the lower electronegativity of selenium, the **FBSe** unit actually possesses a higher dipole moment (Fig. S4†) for the stronger intermolecular interaction.[46] Therefore, in the case of **P2**, the low **FBSe** content enhanced the interchain interaction and consequently increased the π-stacking diffraction intensity. A further increase in the **FBSe** content resulted in an even stronger π-stacking diffraction and a shorter $d_{\pi-\pi}$ of **P1**. Therefore, the π-stacking order of the **FBSe** : FBT copolymers was affected both by the steric effect and the strength of the intermolecular interaction.

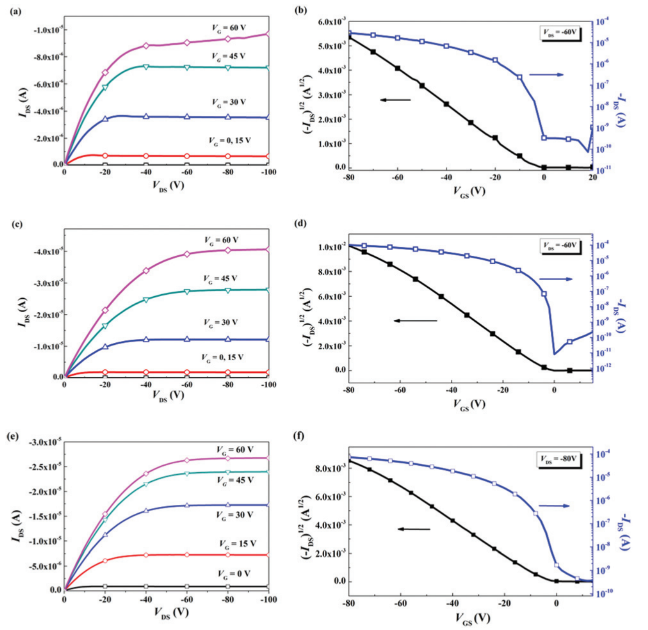

Fig. 3 Typical output curves (a, c, e) and transfer plots (b, d, f) of the OFET devices based on **PTh$_4$FBSe**, **P1**, and **P2**, respectively.

Table 2 OFET characteristics of polymers

Polymer	Annealing temp. (°C)	Mobility (cm^2 V^{-1} s^{-1})	I_{on}/I_{off}	V_{th} (V)
PTh$_4$FBSe	200	0.12	9.19×10^5	−3.4
P1	200	0.46	1.24×10^7	−4.4
P2	250	0.32	9.19×10^6	−5.7

OFET performances

The charge transport properties of the **FBSe** : FBT copolymers were investigated in OFET devices with a bottom-gate, top-contact configuration. The output and transfer plots of the devices exhibited typical p-channel OFET characteristics (Fig. 3). The hole mobilities (μ_hs) of the copolymers were obtained from the transfer characteristics of the devices in the saturation regime (Table 2). The μ_hs of **PTh$_4$FBSe**, **P1** and **P2** were 0.12, 0.46, and 0.32 cm^2 V^{-1} s^{-1}, respectively. It was found that the μ_hs of the copolymers have better correlation with the π-stacking order than the lamellar order. **P1**, which has the highest π-stacking order and the shortest $d_{\pi-\pi}$, but the lowest lamellar order, delivered the highest μ_h (0.46 cm^2 V^{-1} s^{-1}) among the copolymers. Remarkably, the μ_h of the random copolymer **P1** is higher than the μ_hs of regular alternating copolymers, **PTh$_4$FBSe** (0.12 cm^2 V^{-1} s^{-1}) and **PTh$_4$FBT** (0.29 cm^2 V^{-1} s^{-1}).[46] The observation is not trivial, because it has been known that the lack of backbone regularity degraded the solid-state order and therefore the charge mobility of the conjugated polymers.[51] **P1** provides an important example showing that although the lack of backbone regularity degrades the lamellar order, the adjustment of the **FBSe** : FBT ratio enables the optimization of the π-stacking order and the μ_hs of the copolymers.

BHJ PSC characteristics

To evaluate the photovoltaic performances of the copolymers, BHJ PSCs with an inverted architecture – ITO/ZnO/copolymer : PC$_{71}$BM (1 : 2 w/w)/MoO$_3$/Ag were fabricated. The current density–voltage characteristics of the devices under a simulated AM 1.5 G illumination of 100 mW cm^{-2} are shown in Fig. 4 and summarized in Table 3. Without optimization, V_{oc} and J_{sc} were 0.68 V, and 11.9 mA cm^{-2}, respectively, for the **PTh$_4$FBSe** PSCs; 0.68 V, and 11.4 mA cm^{-2} for the **P1** PSCs, respectively; and 0.72 V and 10.5 mA cm^{-2} for the **P2** PSCs, respectively. The external quantum efficiency (EQE) measurements of the PSCs are shown in Fig. 5. Without DIO additive, **PTh$_4$FBSe** : PC$_{71}$BM PSCs delivered an EQE value which exceeds 40% over the wavelength range from 380 nm to 740 nm, but the EQE values of the **P1** : PC$_{71}$BM and **P2** : PC$_{71}$BM PSCs are lower in the same range. The results explain the highest J_{sc} of 11.9 mA cm^{-2} delivered by the **PTh$_4$FBSe** : PC$_{71}$BM PSCs. Although the EQE values of the **P1** : PC$_{71}$BM and **P2** : PC$_{71}$BM PSCs are similar in the wave-

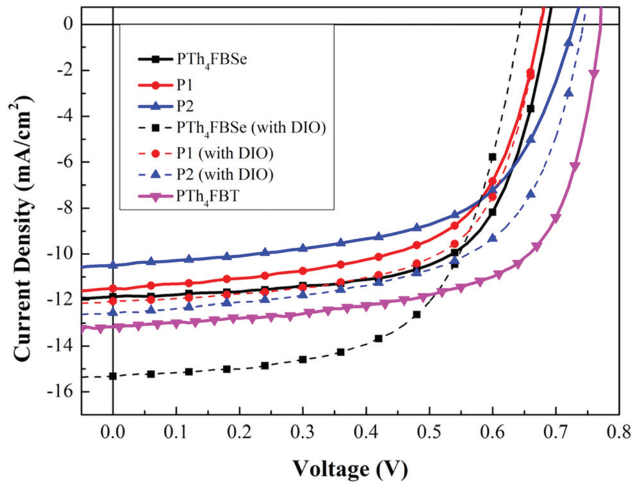

Fig. 4 Current density–voltage characteristics of the copolymer: PC$_{71}$BM BHJ PSCs in inverted device architectures under illumination of AM 1.5 G at 100 mW cm^{-2}.

Table 3 PSC characteristics of the polymer : PC$_{71}$BM BHJ PSCs

Polymer/PC$_{71}$BM (w/w; 1 : 2)	V_{oc} (V)	J_{sc} (mA cm^{-2})	FF (%)	PCE$_{max}$/PCE$_{avg}$[b] (%)
PTh$_4$FBSe	0.68	11.9	66.5	5.38/5.30
P1	0.68	11.4	60.5	4.70/4.54
P2	0.72	10.5	59.3	4.48/4.29
PTh$_4$FBSe[a]	0.64	15.3	61.8	6.06/6.04
P1[a]	0.68	12.0	64.1	5.20/5.16
P2[a]	0.74	12.6	60.6	5.63/5.56

[a] With 3 vol% of DIO as an additive. [b] The average value of 15 devices.

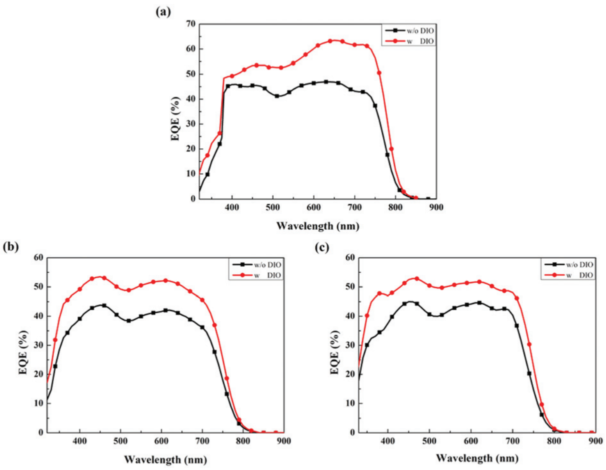

Fig. 5 External quantum efficiency (EQE) spectra of (a) **PTh$_4$FBSe** : PC$_{71}$BM, (b) **P1** : PC$_{71}$BM, and (c) **P2** : PC$_{71}$BM BHJ PSCs prepared with and without 3 vol% of DIO.

length range from 300 nm to 700 nm, the onset of the **P2** : PC$_{71}$BM device is at 761 nm, but that of the **P1** : PC$_{71}$BM device is at 790 nm. The extra photons in the longer wavelength region harvested by **P1** contributed to the higher J_{sc} of the **P1** : PC$_{71}$BM device. Thus, the higher **FBSe** content in **PTh$_4$FBSe** and **P1** led to the narrower E_gs of the copolymers and the higher J_{sc}s of the devices. In contrast, the higher FBT content in **P2** resulted in a lower-lying E_{HOMO} and a higher V_{oc}.

However, when compared to the J_{sc} of **PTh$_4$FBT** : PC$_{71}$BM PSCs (13.5 mA cm^{-2}),[46] the narrower E_g of **PTh$_4$FBSe** did not promote a higher J_{sc}. To identify the origins of the low J_{sc}, the morphology of the active layers was investigated using HR-TEM. As shown in Fig. 6a, c and e, the copolymer : PC$_{71}$BM thin-films are very homogeneous, regardless of the **FBSe** : FBT ratios of the copolymers. The images suggested that the copolymers have good miscibility in PC$_{71}$BM. These overly homogeneous blends may cause insufficient phase separation and fragmented charge transporting channels. Hence, DIO was used as a process additive to promote the phase segregation.[52,53] With 3 vol% of DIO, the enhanced contrast in the **PTh$_4$FBSe** : PC$_{71}$BM thin film (Fig. 6b) indicates a more obvious separation between **PTh$_4$FBSe** and PC$_{71}$BM. The interpenetrating **PTh$_4$FBSe**-rich, and PC$_{71}$BM-rich domains became relatively larger and were beneficial for charge transport. The hole mobilities of the **PTh$_4$FBSe** : PC$_{71}$BM blend films under a space charge limited current (SCLC) model increased from 6.73×10^{-4} cm^2 V^{-1} s^{-1} for the devices prepared without DIO to 3.38×10^{-3} cm^2 V^{-1} s^{-1} for those prepared with DIO, indicating that the enhanced phase separation improved the charge mobility. Furthermore, the EQE values of the **PTh$_4$FBSe** : PC$_{71}$BM PSCs increased from 40% (Fig. 5a, without DIO) to over 50% (Fig. 5a, with DIO) in the wavelength range from 380 nm to 770 nm. Thus, because of the morphological change, the J_{sc} of the **PTh$_4$FBSe** : PC$_{71}$BM PSCs (Fig. 5a) increased correspondingly from 11.9 to 15.3 mA cm^{-2} to give a PCE of 6.06%. However, DIO did not cause significant morphological changes in the **P1** : PC$_{71}$BM and **P2** : PC$_{71}$BM active layers as shown in the TEM images (Fig. 6d, f). It is possible that the random ternary copolymers have better miscibility in PC$_{71}$BM, so that the DIO additive has less effect on the degree of phase separation. The J_{sc}s of the **P1** : PC$_{71}$BM and **P2** : PC$_{71}$BM PSCs increased slightly to 12.0 mA cm^{-2} and 12.6 mA cm^{-2}, respectively, to deliver PCEs up to 5.20% and 5.63% (Table 3).

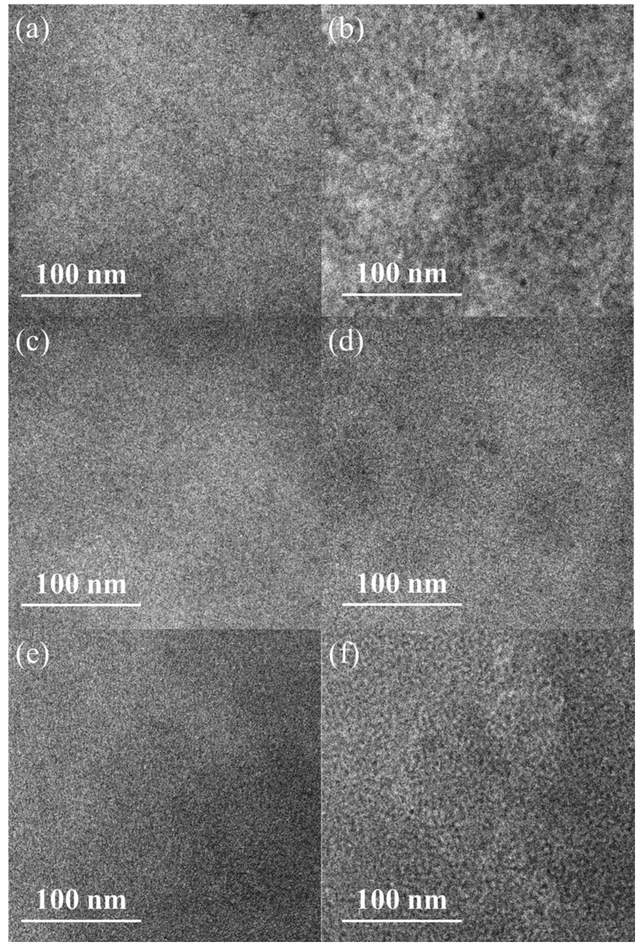

Fig. 6 HR-TEM images of (a) **PTh$_4$FBSe** : PC$_{71}$BM (1 : 2 in wt%); (b) **PTh$_4$FBSe** : PC$_{71}$BM (1 : 2 in wt%) with 3 vol% of DIO; (c) **P1** : PC$_{71}$BM (1 : 2 in wt%); (d) **P1** : PC$_{71}$BM (1 : 2 in wt%) with 3 vol% of DIO; (e) **P2** : PC$_{71}$BM (1 : 2 in wt%); (f) **P2** : PC$_{71}$BM (1 : 2 in wt%) with 3 vol% of DIO thin films prepared from a CB solution.

Conclusions

In this study a series of D–A copolymers containing different **FBSe** : FBT ratios were synthesized. The influences of the **FBSe** : FBT ratio on the polymer properties, solid-state morphology and device performances were investigated. It was found that the copolymers with higher **FBSe** content have narrower E_g, higher lying E_{HOMO}, and delivered higher J_{sc}, but lower V_{oc} in the PSCs. DSC results indicated that **P1**, which has the most irregular **FBSe** : FBT sequence along the backbone showed the lowest T_m. XRD results showed that the solid-state packing of the copolymers is affected by the chain sequence, steric effect of the chalcogen atoms (Se *vs.* S) and the intermolecular interaction strength. However, it is interesting to find that the irregularity in the chain sequence degrades the lamellar order, but not the π-stacking order. The random ternary copolymers, **P1** and **P2**, possess more ordered π-stacking than the alternating copolymers, **PTh$_4$FBSe** and **PTh$_4$FBT**. The most irregular **P1** even has the smallest $d_{\pi-\pi}$ among all the **FBSe** : FBT copolymers. Thus, **P1** delivered the highest OFET μ_h of 0.46 $cm^2\ V^{-1}\ s^{-1}$ because of its ordered π-stacking and small $d_{\pi-\pi}$. In the polymer : $PC_{71}BM$ blend films, the **FBSe** containing copolymers have good miscibility in $PC_{71}BM$. The degree of phase separation of **PTh$_4$FBSe** : $PC_{71}BM$ can be enhanced by DIO additive, but it is not effective for the random ternary copolymers. The highest PCE of 6.06 % with V_{oc} of 0.64 V, J_{sc} of 15.3 mA cm^{-2}, and FF of 61.8% was delivered by the **PTh$_4$FBSe** : $PC_{71}BM$ PSCs. Because the **FBSe** and FBT units are very similar in their structures, the influences of the acceptor ratios and the backbone randomness were better identified in this study.

Acknowledgements

This work was supported by the Ministry of Science and "ATP" project of the National Chiao Tung University and Ministry of Education, Taiwan.

References

1 Y.-J. Cheng, S.-H. Yang and C.-S. Hsu, *Chem. Rev.*, 2009, **109**, 5868.
2 L. Lu and L. Yu, *Adv. Mater.*, 2014, **26**, 4413.
3 Y. Li, *Acc. Chem. Res.*, 2012, **45**, 723.
4 L. Dou, J. You, Z. Hong, Z. Xu, G. Li, R. A. Street and Y. Yang, *Adv. Mater.*, 2013, **25**, 6642.
5 J.-S. Wu, S.-W. Cheng, Y.-J. Cheng and C.-S. Hsu, *Chem. Soc. Rev.*, 2015, **44**, 1113.
6 H. Zhong, Z. Li, F. Deledalle, E. C. Fregoso, M. Shahid, Z. Fei, C. B. Nielsen, N. Yaacobi-Gross, S. Rossbauer, T. D. Anthopoulos, J. R. Durrant and M. Heeney, *J. Am. Chem. Soc.*, 2013, **135**, 2040.
7 S. Zhang, L. Ye, W. Zhao, D. Liu, H. Yao and J. Hou, *Macromolecules*, 2014, **47**, 4653.
8 Y.-X. Xu, C.-C. Chueh, H.-L. Yip, F.-Z. Ding, Y.-X. Li, C.-Z. Li, X. Li, W.-C. Chen and A. K.-Y. Jen, *Adv. Mater.*, 2012, **24**, 6356.
9 J. Subbiah, B. Purushothaman, M. Chen, T. Qin, M. Gao, D. Vak, F. H. Scholes, X. Chen, S. E. Watkins, G. J. Wilson, A. B. Holmes, W. W. Wong and D. J. Jones, *Adv. Mater.*, 2015, **27**, 702.
10 H. J. Son, L. Lu, W. Chen, T. Xu, T. Zheng, B. Carsten, J. Strzalka, S. B. Darling, L. X. Chen and L. Yu, *Adv. Mater.*, 2013, **25**, 838.
11 I. Osaka, T. Kakara, N. Takemura, T. Koganezawa and K. Takimiya, *J. Am. Chem. Soc.*, 2013, **135**, 8834.
12 C. B. Nielsen, R. S. Ashraf, N. D. Treat, B. C. Schroeder, J. E. Donaghey, A. J. P. White, N. Stingelin and I. McCulloch, *Adv. Mater.*, 2015, **27**, 948.
13 T. L. Nguyen, H. Choi, S. J. Ko, M. A. Uddin, B. Walker, S. Yum, J.-E. Jeong, M. H. Yun, T. J. Shin, S. Hwang, J. Y. Kim and H. Y. Woo, *Energy Environ. Sci.*, 2014, **7**, 3040.
14 J.-H. Kim, M. Lee, H. Yang and D.-H. Hwang, *J. Mater. Chem. A*, 2014, **2**, 6348.
15 Z. He, C. Zhong, S. Su, M. Xu, H. Wu and Y. Cao, *Nat. Photonics*, 2012, **6**, 591.
16 L. Dou, C.-C. Chen, K. Yoshimura, K. Ohya, W.-H. Chang, J. Gao, Y. Liu, E. Richard and Y. Yang, *Macromolecules*, 2013, **46**, 3384.
17 C.-Y. Chang, Y.-J. Cheng, S.-H. Hung, J.-S. Wu, W.-S. Kao, C.-H. Lee and C.-S. Hsu, *Adv. Mater.*, 2012, **24**, 549.
18 C. Cabanetos, A. El Labban, J. A. Bartelt, J. D. Douglas, W. R. Mateker, J. M. Frechet, M. D. McGehee and P. M. Beaujuge, *J. Am. Chem. Soc.*, 2013, **135**, 4656.
19 Y.-H. Chao, J.-F. Jheng, J.-S. Wu, K.-Y. Wu, H.-H. Peng, M.-C. Tsai, C.-L. Wang, Y.-N. Hsiao, C.-L. Wang, C.-Y. Lin and C.-S. Hsu, *Adv. Mater.*, 2014, **26**, 5205.
20 Z. Zhu, D. Waller, R. Gaudiana, M. Morana, D. Mühlbacher, M. Scharber and C. Brabec, *Macromolecules*, 2007, **40**, 1981.
21 J. Li, K.-H. Ong, P. Sonar, S.-L. Lim, G.-M. Ng, H.-K. Wong, H.-S. Tan and Z.-K. Chen, *Polym. Chem.*, 2013, **4**, 804.
22 K.-H. Kim, S. Park, H. Yu, H. Kang, I. Song, J. H. Oh and B. J. Kim, *Chem. Mater.*, 2014, **26**, 6963.
23 J. Zhou, S. Xie, E. F. Amond and M. L. Becker, *Macromolecules*, 2013, **46**, 3391.
24 P. Shen, H. Bin, L. Xiao and Y. Li, *Macromolecules*, 2013, **46**, 9575.
25 C. B. Nielsen, R. S. Ashraf, B. C. Schroeder, P. D'Angelo, S. E. Watkins, K. Song, T. D. Anthopoulos and I. McCulloch, *Chem. Commun.*, 2012, **48**, 5832.
26 T. E. Kang, H.-H. Cho, H. j. Kim, W. Lee, H. Kang and B. J. Kim, *Macromolecules*, 2013, **46**, 6806.
27 J. W. Jung, F. Liu, T. P. Russell and W. H. Jo, *Energy Environ. Sci.*, 2013, **6**, 3301.
28 J.-M. Jiang, H.-C. Chen, H.-K. Lin, C.-M. Yu, S.-C. Lan, C.-M. Liu and K.-H. Wei, *Polym. Chem.*, 2013, **4**, 5321.
29 C.-H. Chen, Y.-J. Cheng, C.-Y. Chang and C.-S. Hsu, *Macromolecules*, 2011, **44**, 8415.
30 J.-S. Wu, J.-F. Jheng, J.-Y. Chang, Y.-Y. Lai, K.-Y. Wu, C.-L. Wang and C.-S. Hsu, *Polym. Chem.*, 2014, **5**, 6472.
31 M. Shahid, R. S. Ashraf, Z. Huang, A. J. Kronemeijer, T. McCarthy-Ward, I. McCulloch, J. R. Durrant, H. Sirringhaus and M. Heeney, *J. Mater. Chem.*, 2012, **22**, 12817.

32 H. A. Saadeh, L. Lu, F. He, J. E. Bullock, W. Wang, B. Carsten and L. Yu, *ACS Macro Lett.*, 2012, **1**, 361.
33 M. Planells, B. C. Schroeder and I. McCulloch, *Macromolecules*, 2014, **47**, 5889.
34 J. J. Intemann, K. Yao, H.-L. Yip, Y.-X. Xu, Y.-X. Li, P.-W. Liang, F.-Z. Ding, X. Li and A. K.-Y. Jen, *Chem. Mater.*, 2013, **25**, 3188.
35 L. Dou, W. H. Chang, J. Gao, C.-C. Chen, J. You and Y. Yang, *Adv. Mater.*, 2013, **25**, 825.
36 P. Shen, H. Bin, Y. Zhang and Y. Li, *Polym. Chem.*, 2014, **5**, 567.
37 Y. Li, Z. Pan, L. Miao, Y. Xing, C. Li and Y. Chen, *Polym. Chem.*, 2014, **5**, 330.
38 J.-H. Kim, S. A. Shin, J. B. Park, C. E. Song, W. S. Shin, H. Yang, Y. Li and D.-H. Hwang, *Macromolecules*, 2014, **47**, 1613.
39 R. Yang, R. Tian, J. Yan, Y. Zhang, J. Yang, Q. Hou, W. Yang, C. Zhang and Y. Cao, *Macromolecules*, 2005, **38**, 244.
40 J. Hou, M.-H. Park, S. Zhang, Y. Yao, L.-M. Chen, J.-H. Li and Y. Yang, *Macromolecules*, 2008, **41**, 6012.
41 G. L. Gibson, T. M. McCormick and D. S. Seferos, *J. Am. Chem. Soc.*, 2012, **134**, 539.
42 J.-M. Jiang, P. Raghunath, H.-K. Lin, Y.-C. Lin, M. C. Lin and K.-H. Wei, *Macromolecules*, 2014, **47**, 7070.
43 H. Zhou, L. Yang and W. You, *Macromolecules*, 2012, **45**, 607.
44 H. Zhou, L. Yang, A. C. Stuart, S. C. Price, S. Liu and W. You, *Angew. Chem., Int. Ed.*, 2011, **50**, 2995.
45 A. C. Stuart, J. R. Tumbleston, H. Zhou, W. Li, S. Liu, H. Ade and W. You, *J. Am. Chem. Soc.*, 2013, **135**, 1806.
46 J.-F. Jheng, Y.-Y. Lai, J.-S. Wu, Y.-H. Chao, C.-L. Wang and C.-S. Hsu, *Adv. Mater.*, 2013, **25**, 2445.
47 E. Zhou, J. Cong, K. Hashimoto and K. Tajima, *Macromolecules*, 2013, **46**, 763.
48 K.-H. Ong, S.-L. Lim, J. Li, H.-K. Wong, H.-S. Tan, T.-T. Lin, L. C.-H. Moh, J. C. de Mello and Z.-K. Chen, *Polym. Chem.*, 2013, **4**, 1863.
49 C.-F. Huang, J.-Y. Chang, S.-H. Huang, K.-Y. Wu, J.-F. Jheng, W.-T. Chuang, C.-S. Hsu and C.-L. Wang, *J. Mater. Chem. A*, 2015, **3**, 3968–3974.
50 J. Hollinger, P. M. DiCarmine, D. Karl and D. S. Seferos, *Macromolecules*, 2012, **45**, 3772.
51 R. J. Kline, M. D. McGehee, E. N. Kadnikova, J. Liu and J. M. J. Fréchet, *Adv. Mater.*, 2003, **15**, 1519.
52 J. Peet, J. Y. Kim, N. E. Coates, W. L. Ma, D. Moses, A. J. Heeger and G. C. Bazan, *Nat. Mater.*, 2007, **6**, 497.
53 J. K. Lee, W. L. Ma, C. J. Barbec, J. Yuen, J. S. Moon, J. Y. Kim, K. Lee, G. C. Bazan and A. J. Heeger, *J. Am. Chem. Soc.*, 2008, **130**, 3619.

